

Active Disturbance Rejection-Based Speed Control in Model Predictive Control for Induction Machines

Liming Yan, *Student Member, IEEE*, Fengxiang Wang, *Senior Member, IEEE*, Manfeng Dou, *Member, IEEE*, Zhenbin Zhang, *Senior Member, IEEE*, Ralph Kennel, *Senior Member, IEEE* and José Rodríguez, *Fellow, IEEE*

Abstract—Finite set model predictive torque control (FCSMPTC) of induction machines has received widespread attention in recent years due to its fast dynamic response, intuitive concept, and ability to handle nonlinear constraints. However, FCSMPTC essentially belongs to the open-loop control paradigm, and unmatched parameters inevitably cause electromagnetic torque tracking error. In addition, the outer loop (i.e., the speed loop) based on a proportional-integral (PI) regulator cannot achieve optimal control between speed dynamic response and torque tracking error compensation. The traditional control paradigm is abbreviated as PI-MPTC. In order to solve the aforementioned problem, this paper proposes active disturbance rejection-based model predictive torque control (ADR-MPTC). Firstly, the influence mechanism of mismatched parameters on torque prediction error in PI-MPTC is studied, and then the performance of a traditional PI regulator used to compensate for torque prediction error is analyzed. Secondly, this paper introduces several parts of the proposed ADR-MPTC, including the design of the torque prediction error observer, nonlinear prediction error compensation strategies, an enhanced predictive torque control, and a simplified full order flux observer. Finally, PI-MPTC and ADR-MPTC are studied experimentally. The experimental results show that compared with PI-MPTC, ADR-MPTC performs better in dynamic and steady states, and has stronger robustness.

Index Terms—Nonlinear prediction error, model predictive control, induction machine.

I. INTRODUCTION

In recent years, model predictive control (MPC) has been widely used in power electronics and electrical drives because of its flexible design principle and fast dynamic response [1]–[6], which is suitable for highly dynamic servo control systems. Model predictive control can be categorized into continuous control set model predictive control (CCSMPCC) and finite control set model predictive control (FCSMPC).

The work is supported by National Natural Science Foundation of China (NSFC) No.51877207, and partly by the Chilean Research Fund projects FB0008 and 1170167.(Corresponding author: F. Wang)

Liming Yan is with School of Automobile, Chang'an University, Xi'an 710064, China (e-mail:liming123@mail.nwpu.edu.cn)

Fengxiang Wang is with Quanzhou Institute of Equipment Manufacturing, Haixi Institutes, Chinese Academy of Sciences, Jinjiang, 362200 China (email:fengxiang.wang@fjirsm.ac.cn)

Manfeng Dou is with the Department of Electrical Engineering, School of Automation, Northwestern Polytechnical University,Xian 710072, China (e-mail:doumf@nwpu.edu.cn)

Zhenbin Zhang is with the School of Electrical Engineering, Shandong University, Jinan 250061, China (e-mail: zbz@sdu.edu.cn)

Ralph Kennel is with the Institute for Electrical Drive Systems and Power Electronics, Technische Universitaet Muenchen, 80333, Munich, Germany(email:ralph.kennel@tum.de)

José Rodríguez is with Faculty of Engineering, Universidad Andres Bello, Santiago, 8370146, Chile(email:jose.rodriguez@unab.cl)

The main idea of CCSMPC is to obtain a continuous variable voltage vector reference by solving an optimization problem, and to then modulate the voltage vector reference using space vector pulse width modulation (SVPWM). CCSMPC can be classified into generalized predictive control (GPC) and explicit model predictive control (EMPC). Based on the controlled autoregressive integrated moving average model, GPC can achieve optimal control by utilizing model prediction, rolling optimization and online correction [7]. EMPC adopts an offline solution to the optimization problem, and an online lookup table method to overcome large amounts of online computations [8]. FCSMPC selects the optimal voltage vector by means of exhaustion to realize stator current or electromagnetic torque control. Because FCSMPC corresponds with characteristics of power electronic converters with discrete switching states, it has become a popular research topic in various power electronic converters [9], [10].

In electrical drives, FCSMPC can be categorized into finite control set model predictive current control (FCSMPCC) or finite control set model predictive torque control (FCSMPTC) [11]–[13]. The sufficient performance comparisons between FCSMPTC, field-oriented control (FOC) and Direct Torque Control (DTC) are exhibited in [11], [14]. A detailed comparison of current harmonics, torque ripple, and parameter robustness for FCSMPCC and FCSMPTC is presented in [15]. A detailed comparative analysis for FCSMPCC and SVPWM is exhibited in [16], where it is revealed that FCSMPCC has smaller current harmonics at the same switching frequency. In general, FCSMPCC selects only one voltage vector per sampling period, which leads to large current harmonics in steady state [17], [18]. Double vectors in one sampling period are adopted in [19], [20], which obviously improves the steady-state performance. A universal multiple-vector-based model predictive current control is proposed in [21], which further reduces current harmonics.

Another problem that FCSMPC faces is parameter robustness [22]–[24]. It is known that FCSMPC relies heavily on parameters. However, the induction machines stator resistance and rotor resistance are affected by temperature, and mutual inductances are affected by magnetic circuit nonlinearity. In [25], FCSMPCC's current prediction error under mismatched parameters is analyzed for a two-level voltage source inverter. In [26], the influence of mismatched parameters on torque prediction is analyzed, and a torque correction mechanism is proposed to reduce electromagnetic torque ripple.

However, from another perspective, prediction error caused by mismatched parameters can be regarded as a disturbance.

Accordingly, prediction error can be observed and compensated for [27], [28]. In [29], disturbance compensation-based enhanced robust predictive control is proposed to further improve dynamic performance of multilevel flying capacitors inverter with parameters variations. In [30], a flexible-mode FCSMPC based on disturbance rejection method is shown to achieve transient-state and steady-state performance improvements. In [31], linear disturbance observer-based predictive torque control of induction machine drives is proposed to suppress mismatched parameters and load torque disturbances.

In this paper, for prediction torque error caused by mismatched parameters, ADR-MPTC for induction machine drives is proposed to compensate for predictive torque error. This paper is organized as follows. Section II introduces the mathematical model of induction machines and the two-level voltage source inverter (VSI). Section III elaborates on traditional PI-MPTC, including the influence mechanism of mismatched parameters on FCSMPTC, and the performance of the PI regulator in compensating for prediction torque error. Section IV introduces the proposed ADR-MPTC. Section V makes a detailed comparison of PI-MPTC and ADR-MPTC. Section VI summarizes this paper.

II. MATHEMATICAL MODEL OF INDUCTION MACHINE AND VSI

As presented in Fig.1, in stator reference frame, the mathematical model of the three-phase squirrel cage induction machine based on space vector theory can be described as follows [15]:

$$\vec{v}_s = \vec{i}_s R_s + \frac{d}{dt} \vec{\psi}_s \quad (1)$$

$$0 = \vec{i}_r R_r + \frac{d}{dt} \vec{\psi}_r - j\omega_r \vec{\psi}_r \quad (2)$$

$$\vec{\psi}_s = L_s \vec{i}_s + L_m \vec{i}_r \quad (3)$$

$$\vec{\psi}_r = L_r \vec{i}_r + L_m \vec{i}_s \quad (4)$$

where $\vec{\psi}_s$, $\vec{\psi}_r$, \vec{v}_s , \vec{i} and \vec{i}_r represent stator flux linkage vector, rotor flux linkage vector, voltage vector, stator current vector and rotor current vector, respectively. Stator current vector \vec{i}_s is defined as $\vec{i}_s = i_{sa} + i_{sb}e^{j(2\pi/3)} + i_{sc}e^{j(4\pi/3)}$, where i_{sa} , i_{sb} and i_{sc} are the instantaneous values of three-phase stator currents, respectively. R_s , R_r are stator resistance and rotor resistance. L_m , L_s and L_r are mutual inductance, stator inductance and rotor inductance, respectively. ω_r is the electric speed of the induction machine.

The two-level VSI contains six Insulated Gate Bipolar Transistors (IGBT), as displayed in Fig.1(a). S_a represents the switching state of the upper bridge arm's IGBT during a-phase. $S_a = 1$ denotes on, and $S_a = 0$ denotes off. The two-level VSI can produce eight voltage vectors, as indicated in Fig.1(b), where switching states of voltage vector $u_1[100]$ are $S_a = 1$, $S_b = 0$ and $S_c = 0$.

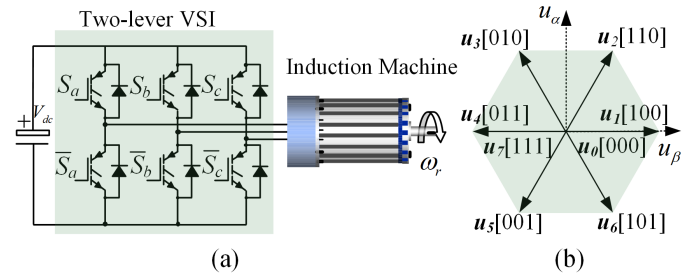


Fig. 1. (a) Two-level VSI and induction machine. (b) Voltage vectors produced by two-level VSI.

III. ANALYSIS OF PI-MPTC WITH PARAMETER MISMATCH

A. Fundamental Principles of PI-MPTC

In traditional PI-MPTC of induction machines, FCSMPTC consists mainly of three parts: the flux observer, torque and flux prediction, and cost function optimization. The speed loop adopts traditional a PI regulator to provide the electromagnetic torque reference for FCSMPTC.

A detailed explanation of PI-MPTC can be found in [11], [15], where the flux observation equations are expressed as (5)-(6), and the prediction equations are presented as (7)-(9).

$$\vec{\psi}_s(k) = \vec{\psi}_s(k-1) + T_s \cdot \vec{v}_s(k-1) - R_s \cdot T_s \cdot \vec{i}_s(k-1) \quad (5)$$

$$\vec{\psi}_r(k) = \frac{L_r}{L_m} \vec{\psi}_s(k) + \vec{i}_s(k) \left(L_m - \frac{L_r L_s}{L_m} \right) \quad (6)$$

$$\begin{aligned} \vec{i}_s(k+1) &= \left(1 - \frac{T_s}{\tau_\sigma} \right) \cdot \vec{i}_s(k) + \frac{T_s}{\tau_\sigma} \frac{1}{R_\sigma} \cdot \\ &\quad \left[k_r \cdot \left(\frac{1}{\tau_r} - j\omega(k) \right) \cdot \vec{\psi}_r(k) + \vec{v}_s(k) \right] \end{aligned} \quad (7)$$

$$\vec{\psi}_s(k+1) = \vec{\psi}_s(k) + T_s \cdot \vec{v}_s(k) - R_s \cdot T_s \cdot \vec{i}_s(k) \quad (8)$$

$$T_e(k+1) = \frac{3}{2} \cdot p \cdot \text{Im} \left\{ \vec{\psi}_s(k+1)^* \cdot \vec{i}_s(k+1) \right\} \quad (9)$$

B. Parameter Mismatch Analysis of MPTC

In order to analyze the effect of mismatched parameters on torque prediction accuracy, the following assumptions are made: (1) $\vec{i}_s(k)$, $\vec{\psi}_r(k)$ and $\vec{\psi}_s(k)$ are the exact values at k sampling time. (2) Stator leakage $L_{s\sigma}$ and rotor leakage $L_{r\sigma}$ are constant. (3) R_s and R_r have the same change rate.

The concrete approach is to assume that R_s , R_r and L_m are actual parameters, and then calculate $\vec{i}_s(k+1)$ and $T_e(k+1)$ according to equations (7)-(9), which can be found in [11], [15]. \tilde{R}_s , \tilde{R}_r and \tilde{L}_m are parameters that are only used in the predictive controller. By altering parameters \tilde{R}_s , \tilde{R}_r , \tilde{L}_m , $\tilde{i}_s(k+1)$ and $\tilde{T}_e(k+1)$ are calculated according to equations (10)-(12). Current prediction error and torque prediction error are defined in terms of $\Delta i_s = |\tilde{i}_s(k+1) - \vec{i}_s(k+1)|$ and $\Delta T_e = |\tilde{T}_e(k+1) - T_e(k+1)|$, respectively. Based on [11], [15], the predictive equations with mismatched parameters are expressed as (10)-(12), where $\tilde{k}_r = \tilde{L}_m / (\tilde{L}_m + L_{r\sigma})$, $\tilde{\sigma} =$

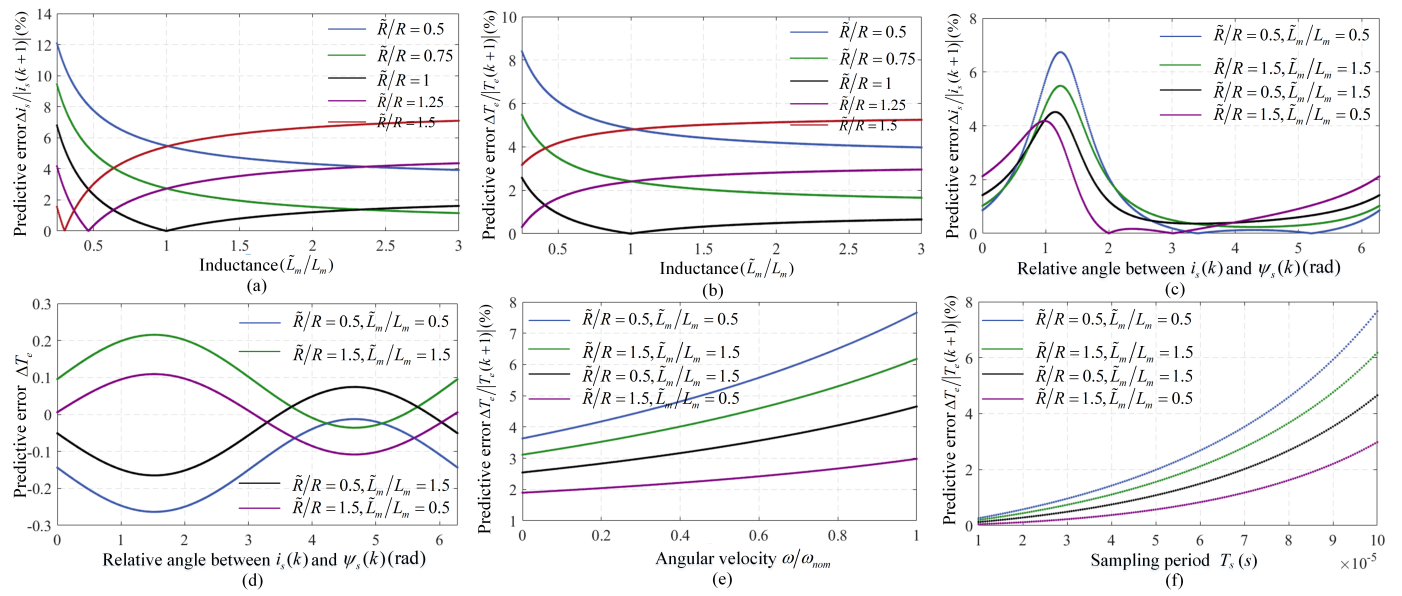


Fig. 2. (a) Predictive error of stator current $i_s(k+1)$ with mismatched \tilde{L}_m and \tilde{R}_s at rated state. (b) Predictive error of electromagnetic torque $T_e(k+1)$ with mismatched \tilde{L}_m and \tilde{R}_s at rated state. (c) Predictive error of stator current $i_s(k+1)$ with different relative angle δ of $i_s(k)$ and $\psi_s(k)$. (d) Predictive error of electromagnetic torque $T_e(k+1)$ with different relative angle δ of $i_s(k)$ and $\psi_s(k)$. (e) Predictive error of electromagnetic torque $T_e(k+1)$ with different angular velocity. (f) Predictive error of electromagnetic torque $T_e(k+1)$ with different sampling periods.

$1 - \left(\tilde{L}_m^2 / (\tilde{L}_m + L_{s\sigma}) \cdot (\tilde{L}_m + L_{r\sigma}) \right)$, $\tilde{R}_\sigma = \tilde{R}_s + \tilde{k}_r^2 \cdot R_r \cdot (\tilde{R}_s / R_s)$, and $\tilde{\tau}_\sigma = \tilde{\sigma} \cdot (\tilde{L}_m + L_{s\sigma}) / \tilde{R}_\sigma$.

$$\tilde{i}_s(k+1) = \left(1 - \frac{T_s}{\tilde{\tau}_\sigma} \right) \cdot \tilde{i}_s(k) + \frac{T_s}{\tilde{\tau}_\sigma} \frac{1}{\tilde{R}_\sigma} \cdot \left[\tilde{k}_r \left(\frac{1}{\tilde{\tau}_r} - j\omega(k) \right) \vec{\psi}_r(k) + \vec{v}_s(k) \right] \quad (10)$$

$$\tilde{\psi}_s(k+1) = \vec{\psi}_s(k) + T_s \cdot \vec{v}_s(k) - \tilde{R}_s \cdot T_s \cdot \vec{i}_s(k) \quad (11)$$

$$\tilde{T}_e(k+1) = \frac{3}{2} \cdot p \cdot \text{Im} \left\{ \tilde{\psi}_s(k+1)^* \cdot \tilde{i}_s(k+1) \right\} \quad (12)$$

Firstly, the influence of \tilde{R}_s and \tilde{L}_m on current prediction and torque prediction at the induction machine's rated state is analyzed. The vectors \vec{i}_s , \vec{i}_r , $\vec{\psi}_s$ and $\vec{\psi}_r$ on the complex plane at rated steady state rotate synchronously, and their relative positions to each other are fixed. For convenience in the present discussion, it is assumed that the direction of $\vec{\psi}_s$ coincides with the a-axis. Based on parameters of induction machine in this paper, $\vec{\psi}_s = 0.91e^{j0}$, $\vec{i}_s = 6.55e^{j(\pi/3)}$ and $\vec{\psi}_r = 1.0291 \cdot \vec{\psi}_s - 0.0162 \cdot \vec{i}_s$ can be obtained. Since a two-level VSI can produce seven different voltage vectors, there are seven different prediction errors. For simplicity, the case of maximum prediction error is selected to be studied in this paper. In Fig.2(a), it is seen that the influence of mismatched \tilde{L}_m on current prediction error is asymmetric. Compared with $\tilde{L}_s/L_s > 1$, mismatched inductance has a more serious impact on current prediction error when $\tilde{L}_s/L_s < 1$. In Fig.2(b), it is seen that the influence of mismatched \tilde{L}_m on torque prediction error is also asymmetric. In the case of $\tilde{R}_s/R_s = 0.5$ and $\tilde{L}_s/L_s = 0.2$, the torque prediction error reaches 8.2%.

In addition, from equations (10)-(12) it can be seen that torque prediction error is related not only to parameters, but also to the included angle δ between $\vec{i}_s(k)$ and $\vec{\psi}_s(k)$. Fig.2(c) shows the effect of mismatched parameters on current prediction error, when the angle δ varies from 0 to 2π . When the angle δ is $\pi/3$ (this is the angle at rated state), current prediction error is maximized. In the case of $\tilde{R}_s/R_s = 0.5$ and $\tilde{L}_s/L_s = 0.5$, current prediction error is at its maximum 6.7%. It is seen that as the angle δ increases, torque prediction error changes periodically. Simultaneously, when the angle is $\pi/3$, mismatched parameters have the greatest influence on torque prediction error.

Torque prediction error is also related to the speed ω_r and sampling period T_s . Fig.2(e) and Fig.2(f) reveal that torque prediction error increases in direct relation to ω_r or T_s increasing.

C. Torque Prediction Error Compensation Analysis of PI controller

For convenience, traditional PI-MPTC can be simplified to the form shown in Fig.3. The FCS-MPTC torque control module can be simplified as $T_e = T_e^* - \Delta T_e$, where ΔT_e is torque prediction error. The measured speed is usually low pass filtered in practical application to attenuate the noise. However, the time constant of low-pass filter is much smaller than that of mechanical system of induction motor. Therefore, in order to analyze conveniently, the low-pass filter is neglected when designing the speed PI controller [32].

Assuming $\Delta T_e = 0$, the transfer function $G_s(s)$, $\omega_m(s)$ divided by $\omega_m^*(s)$, can be expressed as (13). Assuming $\omega^* = 0$, the transfer function $G_d(s)$, $\Delta T_e(s)$ divided by $\omega_m^*(s)$, can be described as (14). The dynamic response of speed ω_m , and the

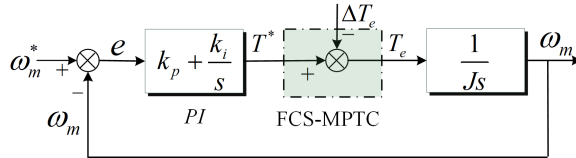


Fig. 3. Block diagram of the speed loop based on proportional-integral controller.

performance of compensating for torque prediction error, both are subject to the denominator $s^2 + (k_p/J)s + (k_i/J)$. Standard form of the denominator can be illustrated as $s^2 + 2\zeta\omega_0 s + \omega_0^2$, where $\zeta = k_p/2\sqrt{Jk_i}$, and $\omega_0 = \sqrt{k_i/J}$. On the other hand, for the integral error (IE), the following formula can be derived as (15).

$$G_c(s) = \frac{\omega_m(s)}{\omega^*(s)}|_{\Delta T_e=0} = \frac{k_p}{J} \frac{s + (k_i/k_p)}{s^2 + (k_p/J)s + (k_i/J)} \quad (13)$$

$$G_d(s) = \frac{\omega_m(s)}{\Delta T_e(s)}|_{\omega^*=0} = -\frac{1}{J} \frac{s}{s^2 + (k_p/J)s + (k_i/J)} \quad (14)$$

$$IE = \int_0^\infty e dt = -\lim_{s \rightarrow 0} G_d(s) \frac{\Delta T_e(s)}{s} = \frac{\Delta T_e(s)}{J} \left(\frac{2\zeta J}{k_p} \right)^2 \quad (15)$$

According to classical control theory, for better compensating for torque prediction error, ζ should be smaller, but if ζ is too small, it can reduce speed dynamic response, and even lead to instability in the system. Therefore, in terms of speed dynamic response and torque prediction error, it must be the tradeoff design.

IV. THE PROPOSED ADR-MPTC

A. Fundamental Principles of ADR-MPTC

In PI-MPTC, torque prediction error is unavoidable due to mismatched parameters. Moreover, the design of the PI regulator requires a tradeoff between speed dynamic response and torque prediction error compensation. In [31], model predictive torque control based on linear disturbance observer and linear compensation strategy is proposed to improve the speed dynamic response of induction machine. Different from this published paper, on the one hand, this paper firstly studies the influence mechanism of mismatched parameters on torque prediction error of induction motor, on the other hand, this paper firstly applies nonlinear compensation based MPC to induction machine drives to compensate the prediction error caused by the mismatched parameters. Hence, this part elaborates on the proposed ADR-MPTC, as presented in Fig.4.

B. Predictive Torque Error Observer and Active Disturbance Rejection Method

The mechanical equation of the induction machine can be expressed as (16). $d(t)$ is the lumped disturbance, given by (17), where J is the moment of inertia for the electrical drive

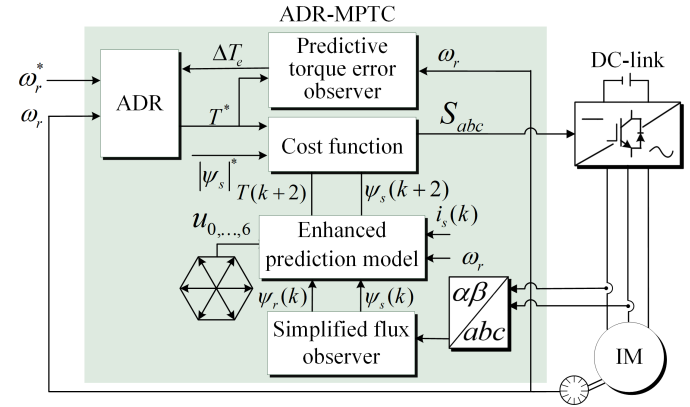


Fig. 4. Block diagram of the proposed ADR-MPTC.

system, and T_L is load torque. B_m and T_f are resistance friction coefficient and Coulomb friction torque, respectively.

$$\dot{\omega}_m = \frac{1}{J} T_e^* + d(t) \quad (16)$$

$$d(t) = \frac{1}{J}(T_e - T_e^*) - \frac{1}{J}(T_L + B_m\omega_m + T_f) \quad (17)$$

Assume $x_1 = \omega_m$, $x_2 = d(t)$, $\dot{x}_2 = g(t)$, $y_2 = x_1$, and system (16) can be expanded into a two-order system (18).

$$\begin{cases} \dot{x}_1 = x_2 + T_e^*/J \\ \dot{x}_2 = g(t) \\ y_2 = x_1 \end{cases} \quad (18)$$

Referring to active disturbance rejection control theory [33], a two-order extended observer equation can be constructed as (19), where $\beta_3 > 0$, $\beta_4 > 0$, $0 \leq \alpha_i \leq 1$, $\delta_i > 0$ and $i = 2, 3$. Suitable parameters α_i , δ_i , β_3 and β_4 can make $z_1 \rightarrow \omega_m$ and $z_2 \rightarrow d(t)$. The nonlinear function $fal(e, \alpha, \delta)$ is defined as (20).

$$\begin{cases} e_2 = x_1 - z_1 \\ \dot{z}_1 = z_2 - \beta_3 fal(e_2, \alpha_2, \delta_2) + T_e^*/J \\ \dot{z}_2 = -\beta_4 fal(e_2, \alpha_3, \delta_3) \end{cases} \quad (19)$$

$$fal(e, \alpha, \delta) = \begin{cases} e/\delta^{1-\alpha} & \text{for } |e| \leq \delta \\ |e|^\alpha \text{sgn}(e) & \text{for } |e| > \delta \end{cases} \quad (20)$$

Hence, the nonlinear control law is designed as (21), where ω^* is speed reference, and $\beta_5 > 0$, $0 \leq \alpha_4 \leq 1$ and $\delta_4 > 0$.

$$T_e^* = \beta_5 fal(\omega^* - z_1, \alpha_4, \delta_4) - Jz_2 \quad (21)$$

Remark I: Nonlinear active disturbance rejection control based on $fal(\cdot)$ is described in detail in [33].

Remark II: When $\alpha < 1$, $fal(e, \alpha, \delta)$ has the characteristics of 'small error and large gain, large error and small gain', which can reduce steady-state error, improve dynamic performance and enhance disturbance rejection ability [33].

Remark III: There are many parameters used in ADRC. The methods of parameter tuning mainly include empirical method, bandwidth method/pole assignment method, artificial intelligence method and practical nonlinear extended state observer parameter tuning equation. In this paper, the empirical method is adopted to tune the parameters. The general principles for

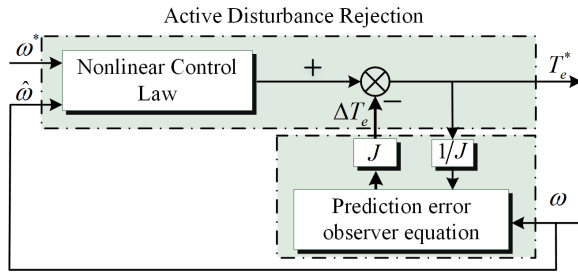


Fig. 5. Block diagram of active disturbance rejection.

selecting extended state observer parameters are as follows: (1) $0 \leq \alpha_i \leq 1, 0.0001 \leq \delta_i \leq 1, i = 2, 3$; (2) the value of $\beta_i (i = 3, 4)$ is determined by tracking performance; (3) If the value of $\delta_i (i = 2, 3)$ is too small, the system will oscillate. Larger $\delta_i (i = 2, 3)$ can improve the tracking performance of extended state observer. In this paper, the parameters of ADRC are set as follows: $\beta_3 = 700, \beta_4 = 5500, \beta_5 = 15, \alpha_2 = \alpha_3 = \alpha_4 = 0.5, \delta_2 = \delta_3 = \delta_4 = 0.01$.

The control principle of traditional PI is to adopt a linear combination of the past and the present forms of the tracking error in order to eliminate the tracking error. However, ADRC achieves the better control performance by using nonlinear combination of the tracking error, which is presented in the equation (21). In addition, ADRC can estimate load disturbance through an extended observer and compensate the load disturbance with a feedforward strategy, which improves the anti-disturbance performance and dynamic response performance of the system.

C. Design of Enhanced FCSMPTC

The mathematical model of the induction machine can be expressed by the following state-space equations:

$$\begin{aligned}\dot{x} &= Ax + Bu \\ i_s &= Cx\end{aligned}\quad (22)$$

where

$$\begin{aligned}\mathbf{x} &= (i_{s\alpha} \ i_{s\beta} \ \psi_{s\alpha} \ \psi_{s\beta})^T, \mathbf{u} = (u_{s\alpha} \ u_{s\beta})^T, \mathbf{i}_s = (i_{s\alpha} \ i_{s\beta})^T \\ \mathbf{B} &= \left[\frac{1}{\sigma L_s} \mathbf{I} \ \mathbf{I} \right]^T, \mathbf{C} = [\mathbf{I} \ \mathbf{0}], \mathbf{I} = \begin{bmatrix} 1 & 0 \\ 0 & 1 \end{bmatrix}, \mathbf{J} = \begin{bmatrix} 0 & -1 \\ 1 & 0 \end{bmatrix}, \\ \mathbf{A} &= \left[-\left(\frac{R_s}{\sigma L_s} + \frac{R_r}{\sigma L_r} \right) \mathbf{I} \ \frac{R_r}{\sigma L_s L_r} \mathbf{I} \right] + \omega_r \left[\mathbf{J} - \frac{1}{\sigma L_s} \mathbf{J} \right], \\ i_{s\alpha} &= \Re \{ \vec{i}_s \}, i_{s\beta} = \Im \{ \vec{i}_s \}, u_{s\alpha} = \Re \{ \vec{v}_s \}, u_{s\beta} = \Im \{ \vec{v}_s \}.\end{aligned}$$

Based on the above equations, the exact discretization mathematical model is as follows:

$$\mathbf{x}(k+1) = e^{AT_s} \mathbf{x}(k) + \left(\int_0^{T_s} e^{A\tau} d\tau \right) \mathbf{B} \mathbf{u}(k) \quad (23)$$

However, equation (23) is too complex to implement in reality. In order to balance accuracy of the discrete model and easy implementation in reality, the following discrete mathematical model is adopted in this paper.

$$\mathbf{x}(k+1) = \Phi \mathbf{x}(k) + \Gamma \mathbf{u}(k) \quad (24)$$

$$\mathbf{i}_s(k+1) = \mathbf{C} \mathbf{x}(k+1) \quad (25)$$

$$\Phi = \mathbf{I} + AT_s + \frac{\mathbf{A}^2 T_s^2}{2}, \Gamma = BT_s + \frac{\mathbf{A}BT_s^2}{2} \quad (26)$$

To compensate for the existing time delay, this paper adopts two-step prediction. The cost function is designed as follows:

$$g = |T_e^* - T_e(k+2)| + \lambda |\Psi_s^* - \Psi_s(k+2)| \quad (27)$$

D. Design of Simplified Full-order Observer

In order to accurately estimate stator flux linkage, a closed-loop linear observer is used, which is described as (28).

$$\dot{\hat{x}} = A\hat{x} + Bu + K(\hat{i}_s - i_s) \quad (28)$$

In traditional gain matrix design, the poles of the observer are directly proportional to those of the induction machine. This ensures the convergence of the observer, but the gain matrix is too complex. In this paper, a simplified gain matrix design is suggested in (29), where $b < 0$. The poles of the induction machine and observer are displayed in Fig.6. It is seen that the designed matrix gain guarantees the convergence of the observer.

$$\mathbf{K} = - \begin{bmatrix} 2b & 0 & \frac{b\sigma L_s L_r}{L_m} & 0 \\ 0 & 2b & 0 & \frac{b\sigma L_s L_r}{L_m} \end{bmatrix}^T \quad (29)$$

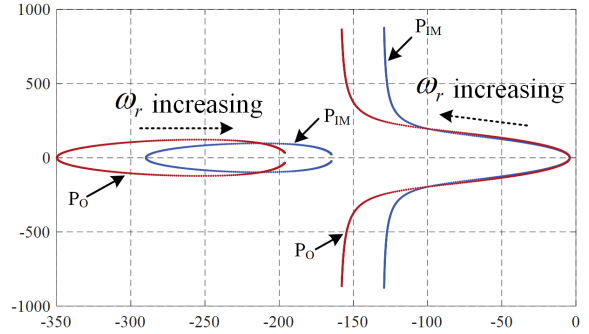


Fig. 6. Pole placements of induction machine and that of a simplified full-order observer. P_{IM} represents pole placement of induction machine, and P_O denotes that of simplified full-order observer.

For the implementation of ADR-MPTC, the overall flow diagram is presented in Fig.7.

V. EXPERIMENTAL EVALUATION

A. Test Bench Description

The proposed ADR-MPTC is verified on the experimental platform illustrated in Fig.8. The experimental platform mainly consists of two induction machines, a Danfoss frequency converter, a Linux real-time control system and a power drive module. In the experiment, the induction machine control system is composed of an induction motor, a power drive module and a Linux real-time system. The algorithm proposed in this paper is implemented in the Linux real-time system. Another induction machine control system is composed of a load motor and a Danfoss frequency converter, which provides load torque. State variables of the induction machine are displayed by oscilloscope.

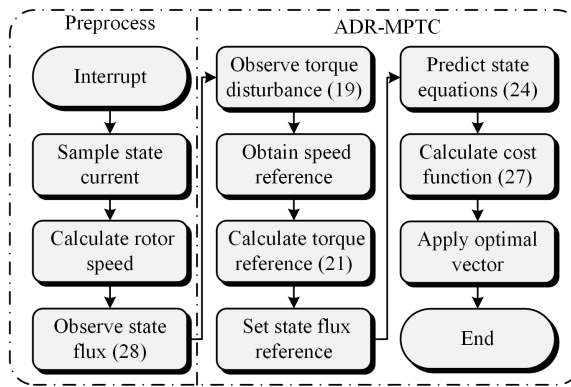


Fig. 7. the overall flow diagram of ADR-MPTC.

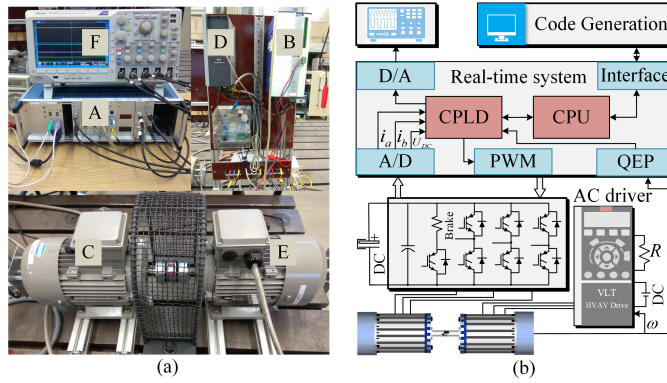


Fig. 8. (a) Test Bench for evaluations, (A) Linux real-time system, (B) Power drive module, (C) Induction machine, (D) Danfoss frequency converter, (E) Induction machine, (F) Oscilloscope. (b) Block diagram of experimental setup.

B. Dynamic-State Performance Comparison

The first test is a dynamic-state performance comparison, including general performance comparison, a comparison of the torque transient response under a step in the torque reference, and a comparison of the speed dynamic response during a step in the load torque.

For showing the advantages, the proposed ADR-MPTC is compared with PI-MPTC. ADR-MPTC adopts the enhanced prediction model which is presented in the equation (24). In the general performance comparison, the speed reference changes from 2772 r/min to -2772 r/min at 0.3 s. For achieving

TABLE I
PARAMETERS OF INDUCTION MACHINE

Descriptions	Parameters	Nominal Values
DC-link Voltage	V_{dc} [V]	582
Rated Speed	ω_{nom} [r/min]	2772
Number of Pole Pairs	p	1.0
Stator Resistance	R_s [Ω]	2.68
Rotor Resistance	R_r [Ω]	2.13
Mutual Inductance	L_m [H]	0.275
Stator Inductance	L_s [H]	0.283
Rotor Inductance	L_r [H]	0.283
Flux Reference	$ \vec{\psi}_s ^*$ [Wb]	0.71

a fair comparison, the same switching frequencies are almost ensured. After observing the average switching frequencies of 3.6 kHz achieved by the proposed improved ADR-MPTC method, the PI parameters of PI-MPTC method are tuned as $k_p = 0.23$ and $k_i = 1.2$ for reaching the same switching frequencies. Fig.9 gave the results based on the above parameters. Compared with PI-MPTC, the settling time of ADR-MPTC is 0.35 s, while that of PI-MPTC speed is 0.62 s, which is 77.14% slower. The proposed ADR-MPTC method has fast dynamics as a main feature. The basic reason is that for PI-MPTC method, the integration part is a slow process for handling transient problem. Therefore, the settling time for the proposed ADR-MPTC is shorter as shown in Fig.9 in the paper. It means that even the values of PI parameters of PI-MPTC are increased, it cannot get the same fast dynamics. Of course, the tuned PI parameters must ensure the speed respond without overshoot. General performance is shown in Fig.10 for PI-MPTC ($k_p = 0.4$, $k_i = 2.0$). The average switching frequencies of these parameters are around 4.3 kHz, which is higher than that in ADR-MPTC method. It is seen that the settling time is still longer than that in ADR-MPTC and with a cost of slight overshoot.

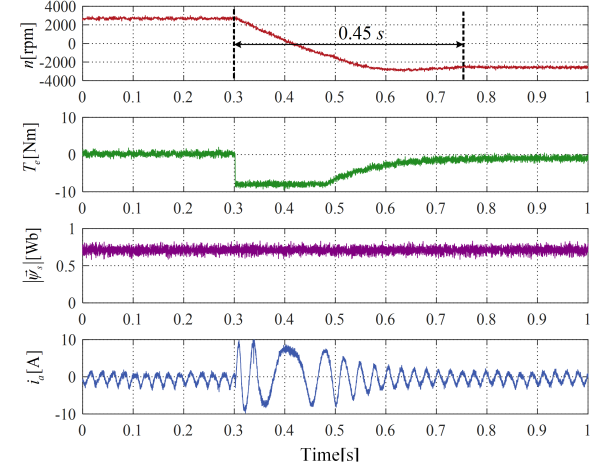


Fig. 10. General performance for PI-MPTC ($k_p = 0.4$, $k_i = 2.0$).

In the electromagnetic torque transient response comparison, the load motor operates in speed mode, and the induction machine operates in torque mode. The torque reference of the induction machine changes from 0 Nm to 7.5 Nm at 4.0 s. The electromagnetic torque responses for ADR-MPTC and PI-MPTC are given in Fig.11. The electromagnetic torque settling time of ADR-MPTC is 590 μ s, while that of PI-MPTC is 800 μ s, which is 33.33% slower. The results are understandable because ADR-MPTC adopts an enhanced prediction model.

In the speed dynamic response comparison, when the induction machine operates at a rated speed of 2772 r/min, load torque 7.5 Nm is suddenly exerted at 2.0 s. The speed dynamic responses of the two algorithms are revealed in Fig.12. The recovery time of ADR-MPTC is 0.82 s, and that of PI-MPTC is 1.57 s, which is 91.46% slower. The torque settling time of ADR-MPTC is 0.10 s, and that of PI-MPTC is 0.37 s, which is 270.0% slower.

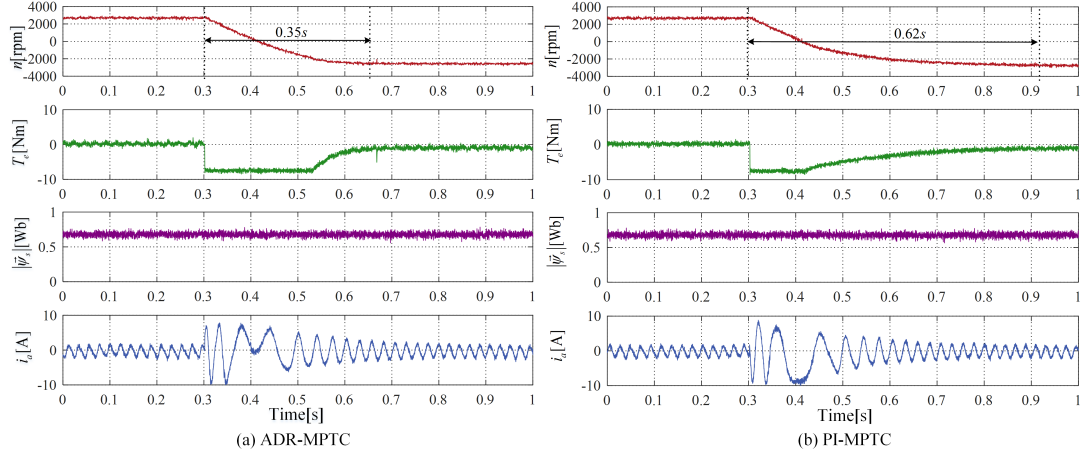


Fig. 9. General performance comparison of induction machine during rated speed reversal process. From up to down are rotor speed n , electromagnetic torque T_e , stator flux magnitude $|\vec{\psi}_s|$ and a-phase stator current i_a , respectively. (a) General performance for ADR-MPTC. (b) General performance for PI-MPTC.

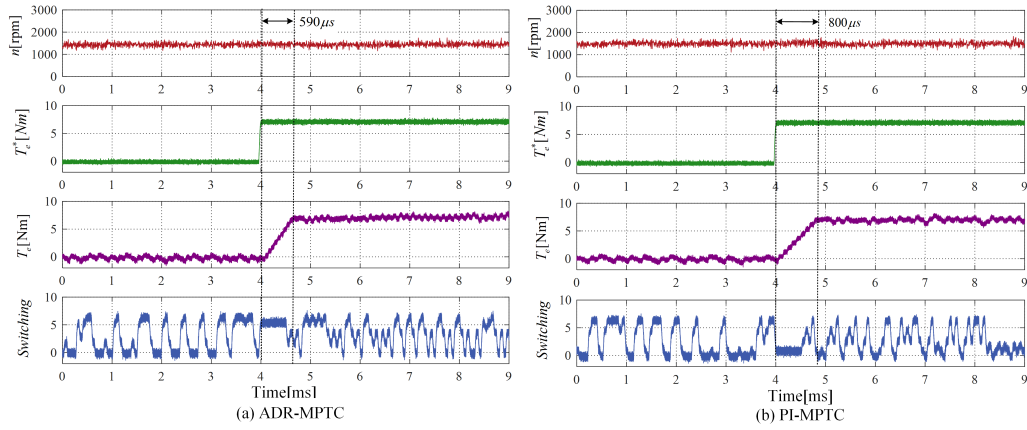


Fig. 11. Transient response comparison of electromagnetic torque for induction machine. From up to down are rotor speed n , electromagnetic torque reference T_e^* , electromagnetic torque transient response T_e and switching vector $u_{opt}(k)$, respectively. (a) Transient response of electromagnetic torque for ADR-MPTC. (b) Transient response of electromagnetic torque for PI-MPTC.

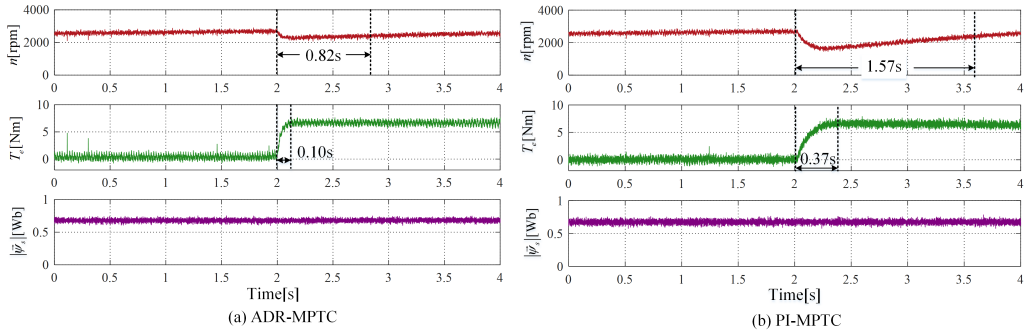


Fig. 12. Dynamic response comparison of rotor speed under step load torque. From up to down are rotor speed n , electromagnetic torque T_e and stator flux magnitude $|\vec{\psi}_s|$, respectively. (a) Dynamic response of rotor speed for ADR-MPTC. (b) Dynamic response of rotor speed for PI-MPTC.

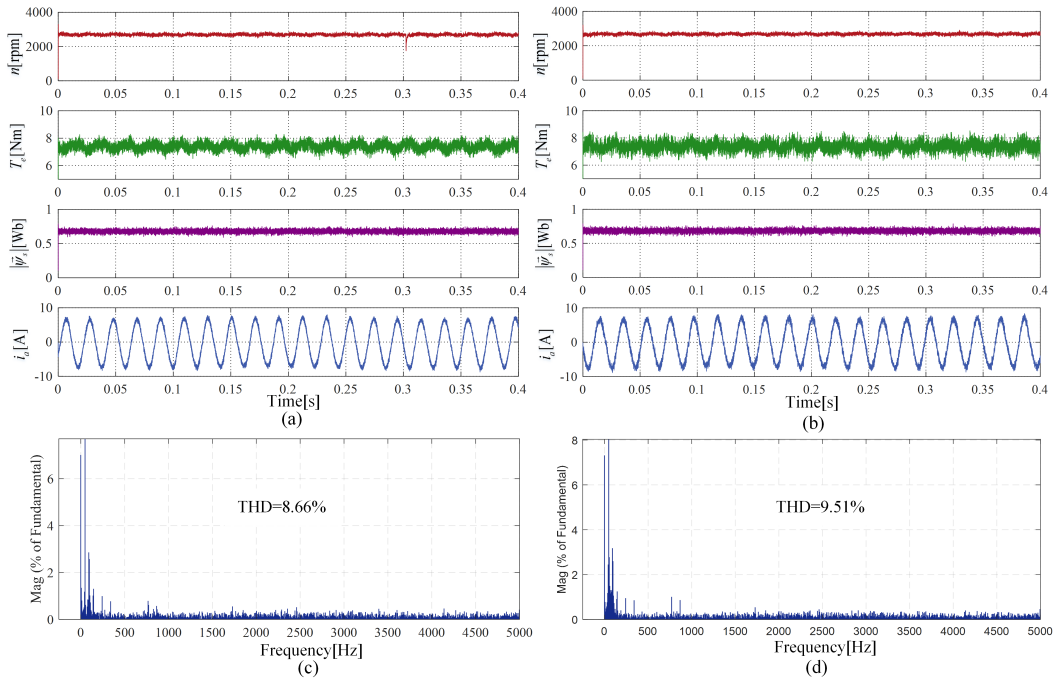


Fig. 13. Steady-state performance comparison at rated state. (a) Steady-state performance for ADR-MPTC. (b) Steady-state performance for PI-MPTC. (c) Stator current harmonic for ADR-MPTC. (d) Stator current harmonic for PI-MPTC.

C. Steady-State Performance Comparison

The second test is a set of comparative experiments of steady-state performance. The reference speed is set to the rated value of 2772 r/min, and load torque is set to the rated value of 7.5 Nm. The speed, electromagnetic torque, stator flux magnitude and stator current waveforms of PI-MPTC and ADR-MPTC are illustrated in Fig.13. It can be seen that the electromagnetic torque ripple of PI-MPTC is about 1.5 Nm, while that of ADR-MPTC is only 1.0 Nm, which is a reduction of 33.33%. The stator current harmonic of PI-MPTC is 9.51%, while that of ADR-MPTC is only 8.66%, which is a reduction of 8.94%.

D. Parameter Sensitivity Comparison

The third test is a parameter sensitivity experiment. In the ADR-MPTC controller of the Linux real-time system, the mismatched stator resistance and mismatched mutual inductance of induction machine are recorded as \tilde{R}_s and \tilde{L}_m , respectively. In this evaluation approach, while the induction machine is operating, the mismatched parameters, \tilde{R}_s and \tilde{L}_m , are linearly increased or decreased in every sampling period until the instability phenomenon of stator current occurs. Fig.14 provides the parameter variation ranges that ensure that the induction machine drives stable for PI-MPTC and ADR-MPTC. It can be seen that stator current under ADR-MPTC will be unstable when \tilde{R}_s increases to 185%, while stator current under PI-MPTC will be unstable when \tilde{R}_s increases to 150%. The mutual inductance variation range to guarantee control system stability is 25%-1100% for ADR-MPTC, and 50%-300% for PI-MPTC. Fig.15 and Fig.16 reveals the robust performance of induction machine drives for PI-MPTC and ADR-MPTC when \tilde{R}_s and \tilde{L}_m change simultaneously. For ADR-MPTC,

stator current will be unstable when \tilde{R}_s increases to 155% and \tilde{L}_m decreases to 45%. For PI-MPTC, stator current will be unstable when \tilde{R}_s increases to 135% and \tilde{L}_m decreases to 60%. In ADR-MPTC, the prediction error caused by the mismatched parameters can be estimated online to compensate for predictive torque control. Therefore, the proposed ADR-MPTC has better robustness than the traditional PI-MPTC. At the same time, the online compensation of the prediction error also improves the dynamic response and reduces the steady state torque ripple.

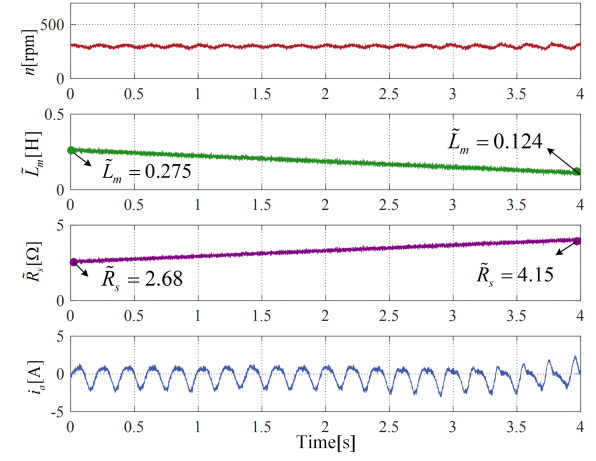


Fig. 15. Robust performance of ADR-MPTC with \tilde{L}_m decreasing and \tilde{R}_s increasing.

E. Summarized Comparison

The experimental results are summarized as follows. From Table II, it can be concluded that the proposed ADR-MPTC

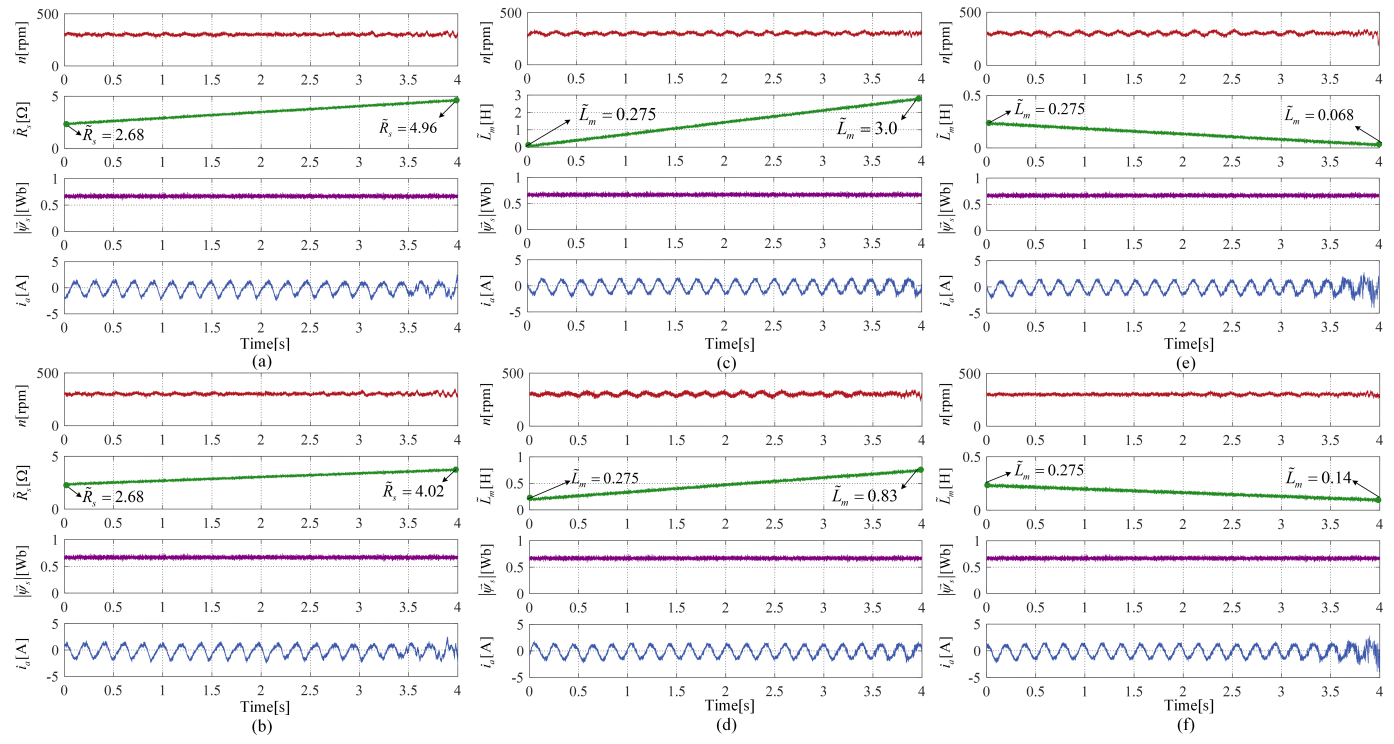


Fig. 14. the parameter sensitivity comparison for mismatched parameters \tilde{R}_s and \tilde{L}_m . From up to down are rotor speed n , electromagnetic torque T_e , mismatched parameter, and a-phase stator current i_a , respectively. (a) Robust performance of ADR-MPTC with \tilde{R}_s increasing. (b) Robust performance of PI-MPTC with \tilde{R}_s increasing. (c) Robust performance of ADR-MPTC with \tilde{L}_m increasing. (d) Robust performance of PI-MPTC with \tilde{L}_m increasing. (e) Robust performance of ADR-MPTC with \tilde{L}_m decreasing. (f) Robust performance of PI-MPTC with \tilde{L}_m decreasing.

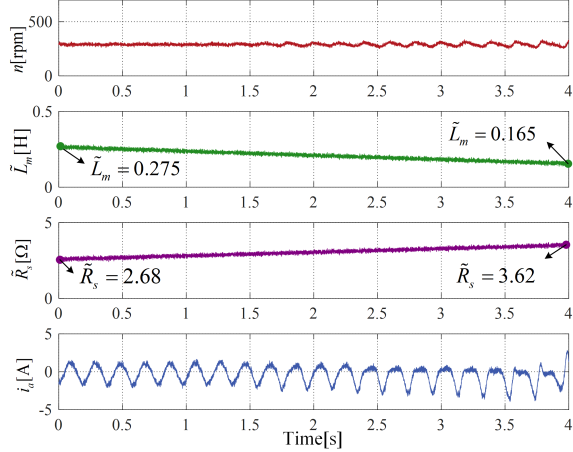


Fig. 16. Robust performance of PI-MPTC with \tilde{L}_m decreasing and \tilde{R}_s increasing.

is superior to traditional PI-MPTC in terms of dynamic performance, steady-state performance and parameter robustness. However, compared with the traditional PI-MPTC, the proposed ADR-MPTC slightly increases the complexity of induction machine drives. Furthermore, for PI-MPTC, in practice, it is also necessary to design complex adaptive parameters in order to enhance the robustness performance.

TABLE II
COMPARISON OF ADR-MPTC AND PI-MPTC

Descriptions	ADR-MPTC	PI-MPTC
ω_{nom} Recovery Time	0.82 s	1.57 s
T_e Settling Time	0.11 s	0.37 s
THD of i_a [%]	8.66%	9.51%
T_{e_ripple}	1.0 Nm	1.5 Nm
\tilde{R}_s Sensitivity Evaluation	185%	150%
\tilde{L}_m Sensitivity Evaluation	25% – 1100%	50% – 300%

VI. CONCLUSION

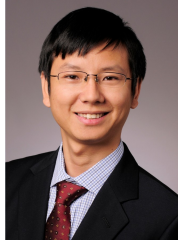
In this paper, ADR-MPTC is proposed to compensate for torque prediction error produced by mismatched parameters. The main contribution of this paper is to analyze the parameter sensitivity of predictive torque control and the anti-disturbance performance of the PI regulator, and then to propose a second-order disturbance observer and a disturbance nonlinear feedforward compensation strategy. Firstly, a nonlinear two-order extended observer is constructed to obtain the predictive torque error. Secondly, a nonlinear control law compensates for the predictive torque error. In addition, an enhanced prediction model and simplified full-order observer further improve prediction accuracy of the electromagnetic torque. The experimental results verify the effectiveness of the proposed algorithm. However, FCSMPTC essentially belongs to hybrid model predictive control. It will be the authors next research topic to analyze and solve electric drive problems based on hybrid model predictive control theory.

REFERENCES

- [1] P. Cortes, M. P. Kazmierkowski, R. M. Kennel, D. E. Quevedo, and J. Rodríguez, "Predictive control in power electronics and drives," *IEEE Transactions on Industrial Electronics*, vol. 55, pp. 4312–4324, Dec. 2008.
- [2] M. Preindl and S. Bolognani, "Model predictive direct torque control with finite control set for pmsm drive systems, part 1: Maximum torque per ampere operation," *IEEE Transactions on Industrial Informatics*, vol. 9, no. 4, pp. 1912–1921, Nov 2013.
- [3] S. Mariethoz, A. Domahidi, and M. Morari, "High-bandwidth explicit model predictive control of electrical drives," *IEEE Transactions on Industry Applications*, vol. 48, no. 6, pp. 1980–1992, Nov 2012.
- [4] P. Antoniewicz and M. P. Kazmierkowski, "Virtual-flux-based predictive direct power control of ac/dc converters with online inductance estimation," *IEEE Transactions on Industrial Electronics*, vol. 55, no. 12, pp. 4381–4390, Dec 2008.
- [5] V. Yaramasu and B. Wu, "Model predictive decoupled active and reactive power control for high-power grid-connected four-level diode-clamped inverters," *IEEE Transactions on Industrial Electronics*, vol. 61, no. 7, pp. 3407–3416, July 2014.
- [6] T. Geyer, "Model predictive direct torque control: Derivation and analysis of the state-feedback control law," *IEEE Transactions on Industry Applications*, vol. 49, pp. 2146–2157, Sep 2013.
- [7] A. A. Ahmed, B. K. Koh, and Y. I. Lee, "A comparison of finite control set and continuous control set model predictive control schemes for speed control of induction motors," *IEEE Transactions on Industrial Informatics*, vol. 14, no. 4, pp. 1334–1346, April 2018.
- [8] S. Bolognani, S. Bolognani, L. Peretti, and M. Zigliotto, "Design and implementation of model predictive control for electrical motor drives," *IEEE Transactions on Industrial Electronics*, vol. 56, no. 6, pp. 1925–1936, June 2009.
- [9] S. Chowdhury, P. W. Wheeler, C. Gerada, and C. Patel, "Model predictive control for a dual-active bridge inverter with a floating bridge," *IEEE Transactions on Industrial Electronics*, vol. 63, no. 9, pp. 5558–5568, Sept 2016.
- [10] M. Vijayagopal, P. Zanchetta, L. Empringham, L. de Lillo, L. Tarisciotti, and P. Wheeler, "Control of a direct matrix converter with modulated model-predictive control," *IEEE Transactions on Industry Applications*, vol. 53, no. 3, pp. 2342–2349, May 2017.
- [11] J. Rodríguez, R. M. Kennel, J. R. Espinoza, M. Trincado, C. A. Silva, and C. A. Rojas, "High-performance control strategies for electrical drives: An experimental assessment," *IEEE Transactions on Industrial Electronics*, vol. 59, no. 2, pp. 812–820, Feb 2012.
- [12] F. Morel, X. Lin-Shi, J. M. Retif, B. Allard, and C. Buttay, "A comparative study of predictive current control schemes for a permanent-magnet synchronous machine drive," *IEEE Transactions on Industrial Electronics*, vol. 56, no. 7, pp. 2715–2728, July 2009.
- [13] O. Sandre-Hernandez, J. Rangel-Magdaleno, and R. Morales-Caporal, "A comparison on finite-set model predictive torque control schemes for pmsm's," *IEEE Transactions on Power Electronics*, pp. 1–1, 2017.
- [14] M. Habibullah, D. D. Lu, D. Xiao, and M. F. Rahman, "Finite-state predictive torque control of induction motor supplied from a three-level npc voltage source inverter," *IEEE Transactions on Power Electronics*, vol. 32, no. 1, pp. 479–489, Jan 2017.
- [15] F. Wang, S. Li, X. Mei, W. Xie, J. Rodríguez, and R. M. Kennel, "Model-based predictive direct control strategies for electrical drives: An experimental evaluation of ptc and pcc methods," *IEEE Transactions on Industrial Informatics*, vol. 11, no. 3, pp. 671–681, June 2015.
- [16] T. Geyer and D. E. Quevedo, "Performance of multistep finite control set model predictive control for power electronics," *IEEE Transactions on Power Electronics*, vol. 30, no. 3, pp. 1633–1644, March 2015.
- [17] R. Morales-Caporal and M. Pacas, "A predictive torque control for the synchronous reluctance machine taking into account the magnetic cross saturation," *IEEE Transactions on Industrial Electronics*, vol. 54, no. 2, pp. 1161–1167, April 2007.
- [18] P. Zanchetta, D. B. Gerry, V. G. Monopoli, J. C. Clare, and P. W. Wheeler, "Predictive current control for multilevel active rectifiers with reduced switching frequency," *IEEE Transactions on Industrial Electronics*, vol. 55, no. 1, pp. 163–172, Jan 2008.
- [19] X. Shi, J. Zhu, L. Li, and D. Lu, "Model predictive based duty-cycle-control with simplified calculation and mutual influence elimination for ac/dc converter," *IEEE Journal of Emerging and Selected Topics in Power Electronics*, pp. 1–1, 2018.
- [20] L. Yan, M. Dou, Z. Hua, H. Zhang, and J. Yang, "Optimal duty cycle model predictive current control of high-altitude ventilator induction motor with extended minimum stator current operation," *IEEE Transactions on Power Electronics*, vol. 33, no. 8, pp. 7240–7251, Aug 2018.
- [21] Y. Zhang, Y. Bai, and H. Yang, "A universal multiple-vector-based model predictive control of induction motor drives," *IEEE Transactions on Power Electronics*, vol. 33, no. 8, pp. 6957–6969, Aug 2018.
- [22] R. P. Aguilera and D. E. Quevedo, "Predictive control of power converters: Designs with guaranteed performance," *IEEE Transactions on Industrial Informatics*, vol. 11, no. 1, pp. 53–63, Feb 2015.
- [23] J. S. Lee and R. D. Lorenz, "Robustness analysis of deadbeat-direct torque and flux control for ipmsm drives," *IEEE Transactions on Industrial Electronics*, vol. 63, no. 5, pp. 2775–2784, May 2016.
- [24] T. Besselmann, J. Lofberg, and M. Morari, "Explicit mpc for lpv systems: Stability and optimality," *IEEE Transactions on Automatic Control*, vol. 57, no. 9, pp. 2322–2332, Sept 2012.
- [25] B. Wang, X. Chen, Y. Yu, G. Wang, and D. Xu, "Robust predictive current control with online disturbance estimation for induction machine drives," *IEEE Transactions on Power Electronics*, vol. 32, no. 6, pp. 4663–4674, June 2017.
- [26] M. Siami, D. A. Khaburi, and J. Rodríguez, "Torque ripple reduction of predictive torque control for pmsm drives with parameter mismatch," *IEEE Transactions on Power Electronics*, vol. 32, no. 9, pp. 7160–7168, Sept 2017.
- [27] J. Wang, F. Wang, G. Wang, S. Li, and L. Yu, "Generalized proportional integral observer based robust finite control set predictive current control for induction motor systems with time-varying disturbances," *IEEE Transactions on Industrial Informatics*, vol. 14, no. 9, pp. 4159–4168, Sep 2018.
- [28] F. Wang, J. Wang, R. Kennel, and J. Rodriguez, "Fast speed control of ac machines without the proportional-integral controller: Using an extended high-gain state observer," *IEEE Transactions on Power Electronics*, pp. 1–1, 2018.
- [29] M. Ghanes, M. Trabelsi, H. Abu-Rub, and L. Ben-Brahim, "Robust adaptive observer-based model predictive control for multilevel flying capacitors inverter," *IEEE Transactions on Industrial Electronics*, vol. 63, no. 12, pp. 7876–7886, Dec 2016.
- [30] H. T. Nguyen and J. W. Jung, "Disturbance-rejection-based model predictive control: Flexible-mode design with a modulator for three-phase inverters," *IEEE Transactions on Industrial Electronics*, vol. 65, no. 4, pp. 2893–2903, April 2018.
- [31] J. Wang, F. Wang, Z. Zhang, S. Li, and J. Rodriguez, "Design and implementation of disturbance compensation-based enhanced robust finite control set predictive torque control for induction motor systems," *IEEE Transactions on Industrial Informatics*, vol. 13, no. 5, pp. 2645–2656, Oct 2017.
- [32] F. Mendoza-Mondragón, V. M. Hernández-Guzmn, and J. Rodríguez-Resendiz, "Robust speed control of permanent magnet synchronous motors using two-degrees-of-freedom control," *IEEE Transactions on Industrial Electronics*, vol. 65, no. 8, pp. 6099–6108, Aug 2018.
- [33] J. Han, "From pid to active disturbance rejection control," *IEEE Transactions on Industrial Electronics*, vol. 56, no. 3, pp. 900–906, March 2009.



Liming Yan (S'18) was born in Shaanxi, China, in 1988. He received the B.S. degree in software engineering at Chang'an University, China, in 2011, and the M.S. degree in electric machine and electric apparatus at Shenyang University of Technology, China, in 2014, and the Ph.D. degree in electrical engineering at Northwestern Polytechnical University, China, in 2019. Currently he is working at Chang'an University, China. His research interests include model predictive control of power electronics and electrical drives.



Fengxiang Wang (S'13-M'14-SM'18) was born in Jiujiang, China, in 1982. He received the B.S. degree in electronic engineering and the M.S. degree in automation from Nanchang Hangkong University, Nanchang, China, in 2005 and 2008, respectively. In 2014, he received Ph.D. degree at the Institute for Electrical Drive Systems and Power Electronics, Technische Universitaet Muenchen, Munich, Germany. Currently he is working at Haixi Institutes, Chinese Academy of Sciences, China. His research interests include predictive control and sensorless control for electrical drives.



Ralph Kennel (M'89-SM'96) was born in Kaiserslautern, Germany, in 1955. He received the Diploma and Dr.-Ing. (Ph.D.) degrees in electrical engineering from the University of Kaiserslautern, Kaiserslautern, in 1979 and 1984, respectively.

From 1983 to 1999, he worked on several positions with Robert BOSCH GmbH, Gerlingen, Germany. Until 1997, he was responsible for the development of servo drives. From 1994 to 1999, he was a Visiting Professor with the University of Newcastle upon Tyne, Newcastle upon Tyne, U.K. From 1999

to 2008, he was a Professor for electrical machines and drives with Wuppertal University (Germany). Since 2008, he has been a Full Professor at the Institute for Electrical Drive systems and Power Electronics, Technische Universität München, Munich, Germany. His main research interests include sensorless control of ac drives, predictive control of power electronics, and hardware-in-the-loop systems.

Dr. Kennel is a Fellow of the Institution of Electrical Engineers and a Chartered Engineer in the U.K. Within the IEEE, he is Treasurer of the Germany Section as well as ECCE Global Partnership Chair of the IEEE Power Electronics Society.



Manfeng Dou (M'08) received the M.S. and Ph.D. degrees in electrical engineering from Northwestern Polytechnical University (NPU), Xian, China, in 1991 and 1998, respectively.

He is currently a Professor with NPU. In addition, he is the Vice Director of the Institute of Rare Earth Permanent Magnet (REPM) Electric Machine and Control Technology, NPU. His research interests include electrical machine design, analysis of electromagnetic fields, motion control technology, and intelligent control.

Dr. Dou received the second prize for the China National Invention Award in 1993, the second prize for the China National Defense Science and Technology Progress Award in 2007, and the Youth Science Award of Shaanxi Province, China, in 2004.



José Rodríguez (M'81-SM'94-F'10) received the Engineer degree in electrical engineering from the Universidad Técnica Federico Santa María, in Valparaíso, Chile, in 1977 and the Dr.-Ing. degree in electrical engineering from the University of Erlangen, Erlangen, Germany, in 1985. He has been with the Department of Electronics Engineering, Universidad Técnica Federico Santa María, since 1977, where he was full Professor and President. Since 2015 he was the President and since 2019 he is full professor at Universidad Andrés Bello in Santiago, Chile. He has coauthored two books, several book chapters and more than 400 journal and conference papers. His main research interests include multilevel inverters, new converter topologies, control of power converters, and adjustable-speed drives. He has received a number of best paper awards from journals of the IEEE. Dr. Rodriguez is member of the Chilean Academy of Engineering. In 2014 he received the National Award of Applied Sciences and Technology from the government of Chile. In 2015 he received the Eugene Mittmann Award from the Industrial Electronics Society of the IEEE.



Zhenbin Zhang (S'13-M'16-SM'18) was born in Shandong, China, in 1984. He received the B.S. degree in electrical engineering and automation from Harbin Engineering University, Harbin, China, in 2008, and the Ph.D. degree (summa cum laude) in electrical engineering from the Institute for Electrical Drive Systems and Power Electronics, Technical University of Munich, Munich, Germany, in 2016.

From 2008 to 2011, he studied control theory and engineering with Shandong University, Jinan, China. From 2016 to 2017, he was a Research Fellow and the team leader for the Modern Control Strategies for Electrical Drives Group with the Institute for Electrical Drive Systems and Power Electronics, Technische Universität München. Since 2017, he has been a Full Professor with Shandong University. His research interests include power electronics and electrical drives, sustainable energy systems, and smart grids.

Dr. Zhang was a recipient of the VDE Award, Suedbayern, Germany, in 2017.